



## OPEN A compact tri-band omnidirectional antenna design for CubeSat applications

Rao Shahid Aziz<sup>1</sup>✉, Slawomir Koziel<sup>1,2</sup> & Anna Pietrenko-Dabrowska<sup>2</sup>

This paper presents a compact tri-band omnidirectional antenna designed for CubeSat applications, operating at UHF (0.755 GHz), L-band (1.25 GHz), and S-band (2.28–3.74 GHz). The antenna features a defected ground structure (DGS) and metallic vias, which enhance impedance matching and enable stable multi-band resonance while maintaining a small footprint of  $0.26\lambda \times 0.26\lambda \times 0.013\lambda$  within a 1U CubeSat. Unlike conventional CubeSat antennas that require external deployment, the proposed design is fully enclosed within the CubeSat, ensuring easy integration and mechanical robustness. The antenna exhibits omnidirectional radiation patterns across all frequency bands, making it suitable for reliable satellite-ground communication. The measured results confirm a high radiation efficiency exceeding 90%, and strong agreement between simulated and experimental results. The combination of compact size, multi-band operation, and high efficiency makes this antenna an ideal candidate for next-generation CubeSat communication systems.

CubeSat is a short term for a Cube Satellite, which is a type of miniaturized satellite that has gained significant popularity in the field of space exploration. CubeSats are also used by commercial enterprises, government and military, and non-profit organizations<sup>1,2</sup>. CubeSats are essentially nanosatellites, which come in different sizes, from 1 to 3U, which means one to three cubes of ten centimeters each side. These little satellites always follow the same size and shape, maintaining 10 cm cube dimensions. Despite their small size, CubeSats can carry various payloads, including cameras, sensors, and scientific instruments. The CubeSat typically weighs between one and 6 kg. The weight of a CubeSat varies depending on factors such as the materials used, the payload it carries, and the specific design considerations. Generally, a 1U CubeSat typically weighs approximately 1 to 1.33 kg, whereas a 3U CubeSat may have a weight ranging from 3 to 4 kg. Larger CubeSats, with configurations beyond 3U, will exhibit correspondingly higher weights<sup>3–10</sup>.

Multiple antennas<sup>11–13</sup>, such as wire antennas (dipole/monopole)<sup>14</sup>, reflector antennas<sup>15</sup>, reflectarray antennas<sup>16</sup>, membrane antennas<sup>17</sup>, horn antennas<sup>18</sup> and patch antennas<sup>19,20</sup> have been devised to meet the requirements of CubeSat systems. However, the deployment structure poses significant challenges during the launch of spacecraft missions. Monopole and dipole antennas are the potential candidates for CubeSat in terms of deployment<sup>10</sup>. Patch antennas are particularly advantageous due to their low profile, lightweight nature, and ability to achieve high gain with miniaturized designs, making them ideal for CubeSat applications<sup>21</sup>. Their planar structure allows for easy integration onto CubeSat surfaces, reducing the need for complex deployment mechanisms<sup>22–24</sup>. Author in<sup>4</sup> presents a simplified design method for single-feed circularly polarized antenna arrays for CubeSats, utilizing circular patches and ring-shaped feed networks. A  $4 \times 4$  RHCP CubeSat downlink array developed using this method achieves over 16.19 dBiC gain with compact dimensions of  $90 \text{ mm} \times 90 \text{ mm}$ . In<sup>7</sup>, a wideband circularly polarized antenna is proposed with a dimension of  $0.48 \lambda_0 \times 0.48 \lambda_0 \times 0.042 \lambda_0$ . It operates at 8 GHz, a wide measured 3-dB axial ratio bandwidth of 98.75% (5.1–13 GHz). In<sup>25</sup>, a circularly polarized antenna has been proposed with the primary radiating element comprising swastika-shaped crossed dipoles. The antenna operates in the L and S-bands within the frequency range of 1.08 to 2.46 GHz. The overall dimensions of the antenna are  $120 \times 120 \times 34.44 \text{ mm}^3$ . It is important to note that this antenna is not deployed in a CubeSat. In<sup>26</sup>, the authors introduced a circularly polarized antenna with cross-dipoles designed for L-Band (1.1–1.6 GHz) satellite communication. The antenna features a radius of 138 mm and a height of 40 mm, achieving a maximum gain of 9 dB. However, it is worth noting that the proposed antenna appears to be bulky, raising considerations about its practical application in a 2U CubeSat at L-band. The authors in<sup>27</sup>, presented two monopole antennas designed for CubeSat applications, operating at frequencies of 149 MHz (VHF) and 398 MHz (UHF). The folded antenna has overall dimensions of  $101 \times 40 \times 8.9 \text{ mm}^3$  when deployed in a CubeSat configuration. The antenna gain is reported as 1.72 dBi at 149 MHz and 3.11 dBi at 398 MHz. Additionally, a

<sup>1</sup>Department of Engineering, Reykjavik University, Reykjavik, Iceland. <sup>2</sup>Faculty of Electronics, Telecommunications and Informatics, Gdansk University of Technology, Gdansk, Poland. ✉email: raos@ru.is

decoupling technique is introduced between the two antennas when installed in a CubeSat, making this design a promising approach, particularly at lower bands. In<sup>28</sup>, the authors proposed a dual-band CubeSat antenna designed to operate in the VHF/UHF frequency bands, specifically tailored for a 1U CubeSat. The dipole antenna utilizes the CubeSat body as a ground plane, aiming to minimize the overall antenna size. However, it is important to note that the antenna is presented in a conceptual form, and its practical realization is pending. The configuration is simulated, revealing a working and lightweight dual-band antenna. Nevertheless, it comes with certain drawbacks, including an asymmetric pattern and the need for a matching network.

Maintaining the confined size and weight of the CubeSat is a great challenge. The CubeSat design specification must also be considered during integration, testing, and servicing of CubeSat. In<sup>29</sup>, a solution to lightweight 1U CubeSat made of plastic material (ABS) for space and educational research has been presented. This technique is less expensive compared to aluminum CubeSat and light in weight. In<sup>30</sup>, the authors fabricated a plastic CubeSat using rapid prototyping and conducted ground-based tests with promising results. Likewise, a dual-band folded-end dipole antenna has been proposed in<sup>9</sup> for plastic CubeSat platforms. Building on this idea, our proposed work also focuses on the weight considerations of the CubeSat. Therefore, we modeled a 1U CubeSat using plastic material manufactured through a 3D printing machine. The antenna, featuring a defected ground plane and metallic strip, is deployed inside the CubeSat, and subjected to testing. The ground plane is surrounded by four metallic strips, each composed of inserted metallic vias and connected to the ground plane. The realized antenna is then deployed within the CubeSat, and both scattering parameters and radiation patterns are tested. The obtained results demonstrate three operational bands: UHF at 0.755 GHz, L-band at 1.25 GHz, and S-band ranging from 2.28 to 3.74 GHz. Additionally, the antenna demonstrates omnidirectional radiation patterns, establishing it as an ideal configuration for satellite communications.

Compared to other published antenna designs for UHF, L, and S bands, the proposed design offers a novel approach with its enhanced stability, compact size, and ease of deployment within a CubeSat. The innovative use of metallic vias and a defected ground structure contributes to the antenna's unique ability to achieve multi-band resonance while maintaining an omnidirectional radiation pattern. Its compact dimensions of  $100 \times 100 \times 101 \text{ mm}^3$ , along with its lightweight nature due to the 3D-printed plastic CubeSat prototyping, maximize space efficiency within the CubeSat, allowing ample room for additional components such as power dividers, amplifiers, and payloads. These dimensions are significantly smaller than those of other state-of-the-art designs, which typically require more space for similar performance. Additionally, the antenna's ability to maintain omnidirectional radiation patterns across all bands ensures reliable communication between space and ground stations, even with dynamic CubeSat orientations. This combination of size reduction, ease of integration, and multi-band functionality represents a significant advancement in CubeSat antenna technology, making it an ideal choice for next-generation satellite communication systems.

## Methods

### Antenna design process

This section introduces and discusses the geometry of the proposed CubeSat antenna design. The antenna is designed and optimized in CST Microwave Studio<sup>31</sup>. First, a stand-alone antenna is designed and optimized. Secondly, it is employed in the CubeSat structure. The following sections explain the development process the proposed CubeSat antenna.

### Antenna geometry

The proposed antenna geometry is shown in Fig. 1. The antenna is designed and optimized in CST Microwave Studio. The antenna consists of metal strips and the ground plane as shown in Fig. 1a and b. The metal strips and the ground plane are designed on Rogers RO4003C (lossy) material, with a relative permittivity of 3.38, a tangent loss of 0.0027, and a thickness,  $d$  of 0.508 mm. The thickness of copper is 0.0175 mm. The metal strips contain vias to ensure the efficient transfer of electrical signals between top and bottom layers as depicted in Fig. 1b. The total of four metal strips are connected to make a square shape. They are also connected to the ground plane through a connecting patch. The distance between the metal strip and antenna ground plane is about 2.2 mm. The antenna is excited by a  $50 \Omega$  coaxial feed line. The distance between the feeding point and the bottom edge of the ground plane is 55 mm as depicted in Fig. 1c. The distance between the grounded patch and the bottom edge of the ground plane is 91 mm as depicted in Fig. 1c.

### Proposed antenna generation methodologies

The evolution of the proposed antenna is explained step by step in this section. The proposed design contains a ground plane and a square-shape metal strip. An extensive study is conducted to elucidate the design methodology implemented in this work.

#### *Antenna with partial metal strips and full ground plane*

The metal strip of the proposed antenna can be divided into two loops i.e., EFGH and IJKL. The geometries of these loops are partially surrounded by a ground plane are shown in Fig. 2. Consider them as two monopoles. The length of loop 1 (EFGH) is about 165 mm. It generates a lower order mode of  $\lambda/2$  at 0.9 GHz and the higher order modes are also generated such as  $\lambda$ ,  $3\lambda/2$ ,  $2\lambda$  and  $5\lambda/2$  (1.8 GHz, 2.7 GHz, and 3.7 GHz) as shown in Fig. 3. Similarly, the length of loop 2 (IJKL) is about 260 mm. It generates lower order mode  $\lambda/2$  at 1.17 GHz and the higher order modes at 2.3 GHz, 2.8 GHz, 3.5 GHz, and 4 GHz. Therefore, after combining loop 1 and 2 they collectively generate UHF standard band at lower resonance (0.82 GHz) and L (1.16 GHz), S (2.3 GHz, 2.6 GHz, 2.9 GHz, 3.5 GHz) resonances at higher bands as shown in Fig. 3. This Figure illustrates the individual and combined S-parameter responses for Loop 1 and Loop 2, which are part of the antenna structure. Loop 1 generates resonances at specific frequencies (0.9 GHz and 1.8 GHz), and Loop 2 contributes to additional



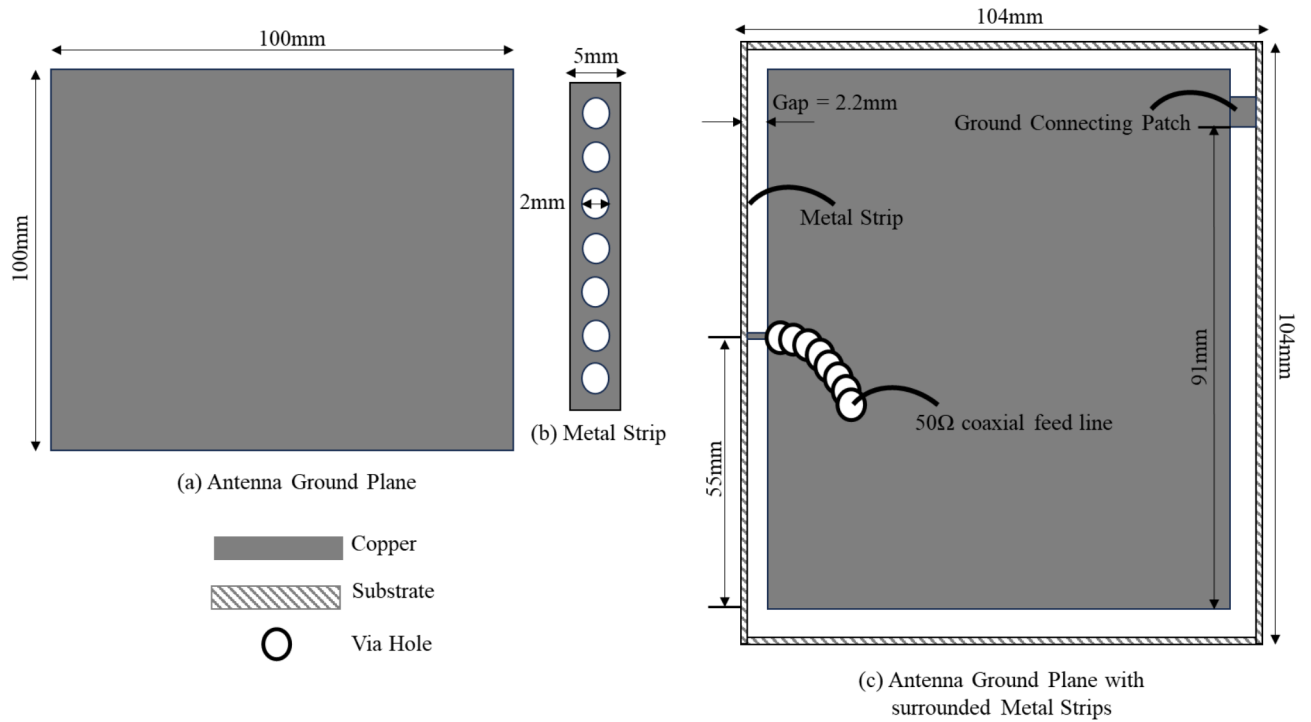


**Fig. 1.** Antenna geometry: (a) ground plane, (b) metal strips with inserted vias, (c) antenna ground plane with surrounding metal strips.

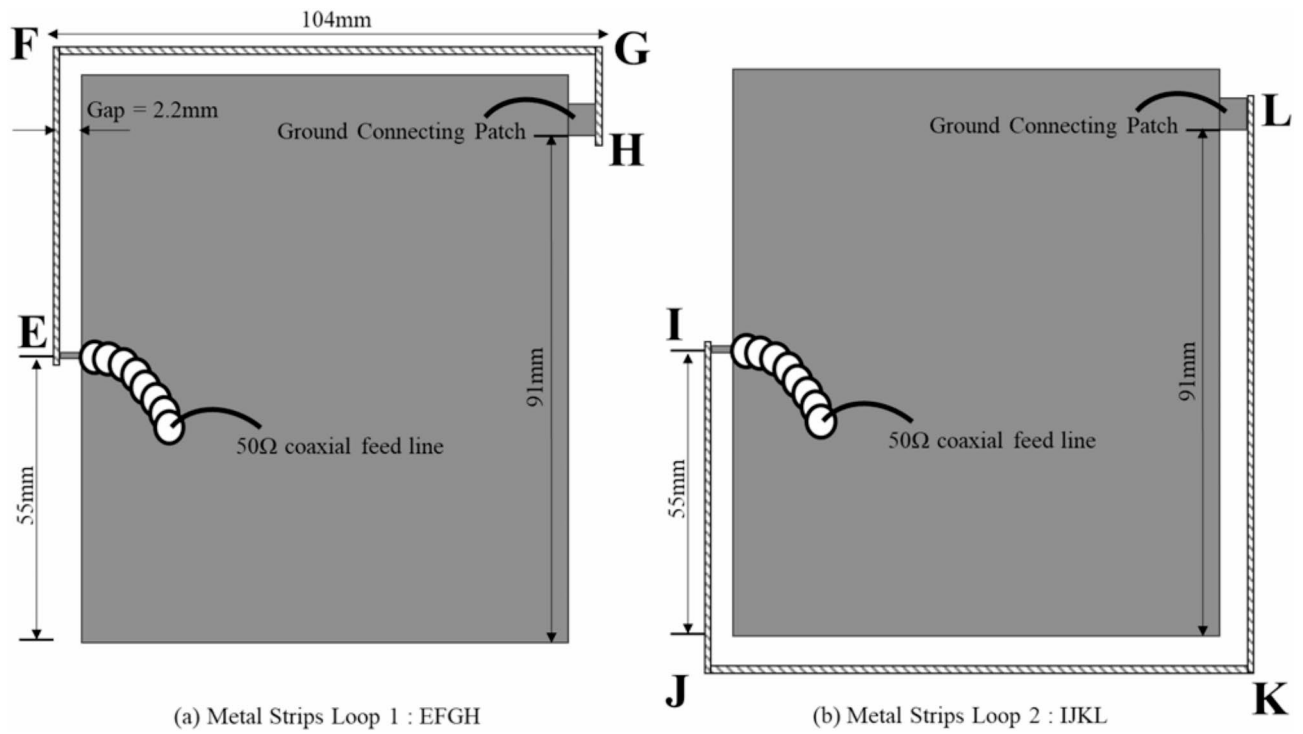


**Fig. 2.** Study of the proposed antenna geometry w.r.t the metal strip: (a) metal strips Loop 1, (b) metal strips Loop 2.

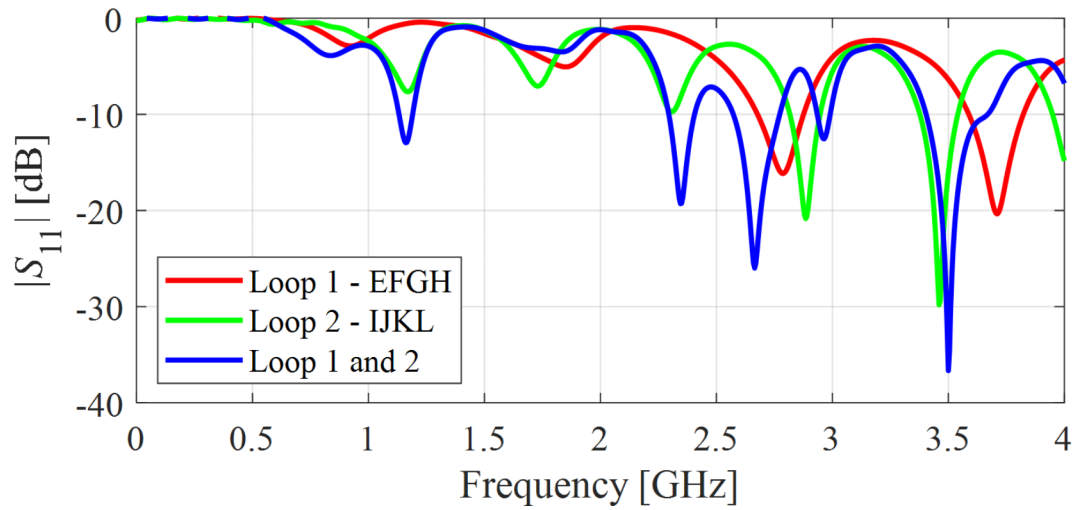


Fig. 3. S-parameters of Loop 1, Loop 2, and their combination.

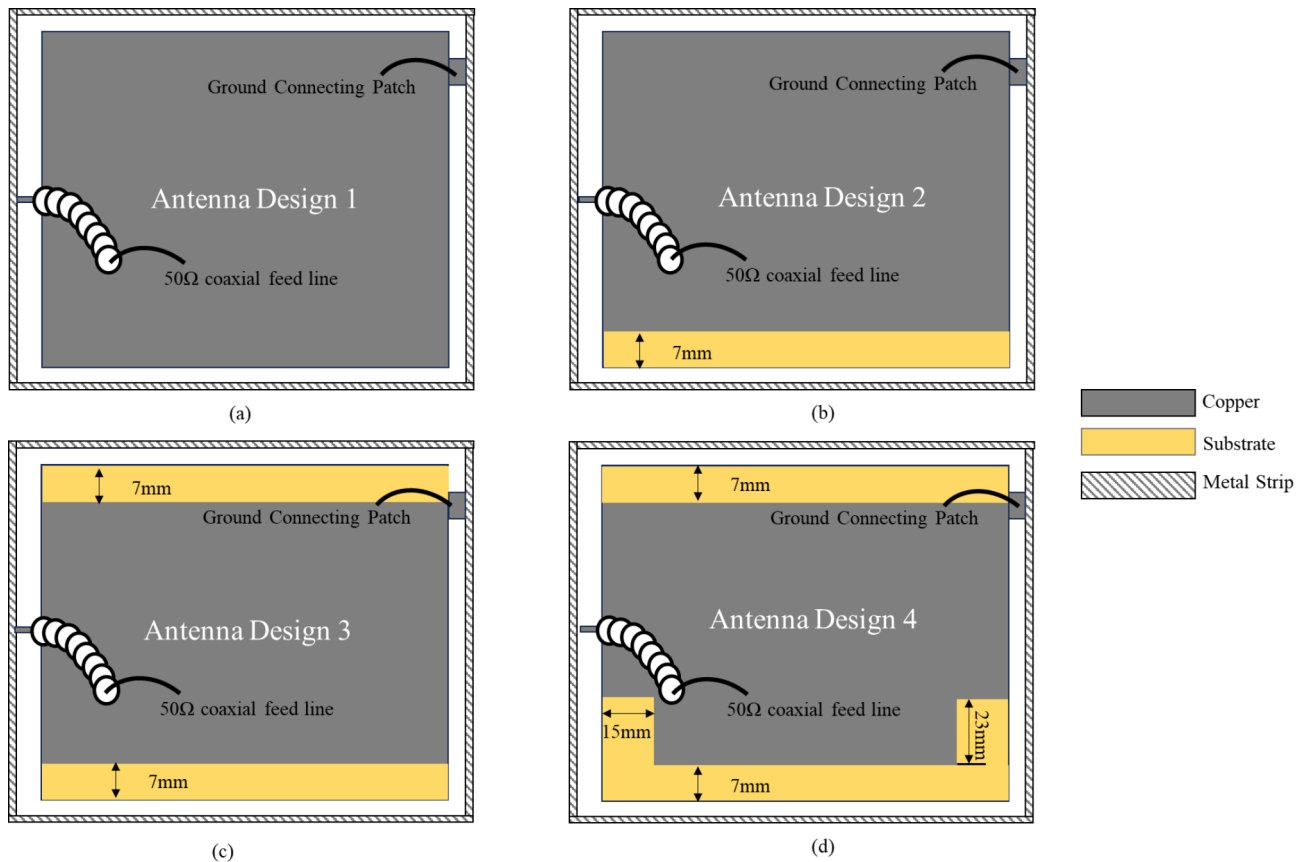
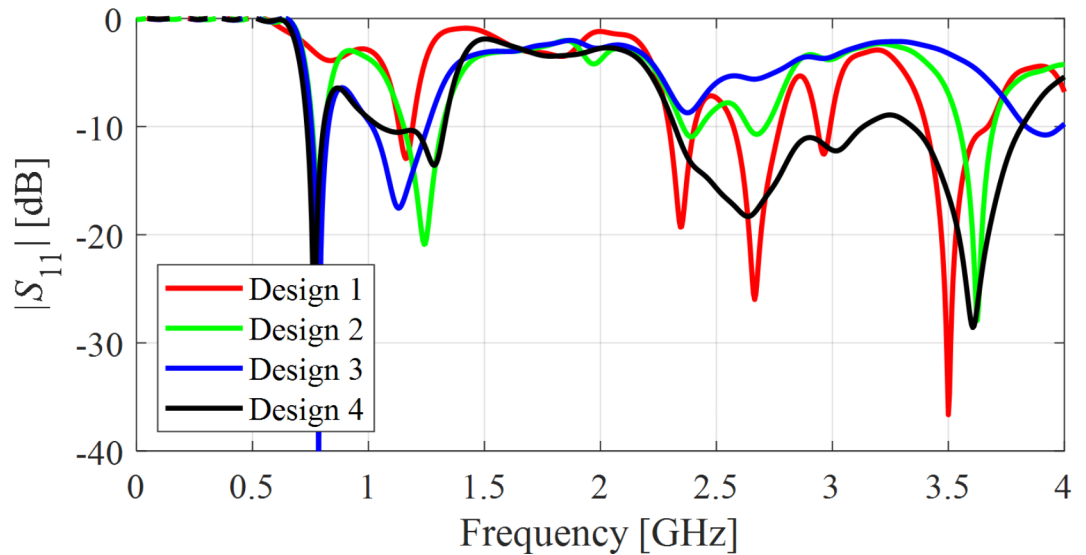


Fig. 4. Study of the proposed antenna geometry w.r.t. the ground plane: (a) Design 1, (b) Design 2, (c) Design 2, (d) Design 4.

resonances (1.17 GHz and higher). When combined, the antenna operates efficiently across UHF, L, and S bands, showing a broad resonance that covers multiple frequencies simultaneously. This combination provides the desired multi-band behavior for CubeSat communication.

*Antenna with full metal strips and partial ground plane*

To further explain the design methodology, consider four evolution steps, referred to as Design 1 through 4, respectively. These designs are depicted in Fig. 4. The objective is to obtain a wide bandwidth to cover as



**Fig. 5.** S-Parameter study of with respect to the ground plane.

Parameters	Size
Size of ground plane	100 × 100 mm <sup>2</sup>
Width of metallic strip	5 mm
Diameter of via	2 mm
Dimension of connecting ground patch	3 × 1.98 mm <sup>2</sup>
Gap between metallic strip and ground plane	2.2 mm
Total area of metallic strip surrounding ground plane	104 × 104 mm <sup>2</sup>
Size of CubeSat	100 × 100 × 100 mm <sup>3</sup>
Distance between feeding point and bottom edge of ground plane	55 mm
Distance between ground connecting patch and bottom edge of ground plane	9 mm

**Table 1.** Optimized parameters of proposed antenna.

many operating bands as possible up to 4 GHz. Design 1 consists of a ground plane, which is connected to the surrounding square shape metal strip. Figure 5 shows its S-parameters. Multi-resonances at lower band (1.1 GHz) and higher bands (2.3 GHz, 2.6 GHz, 2.8 GHz, 3.5 GHz) are obtained. However, these bands are very narrow, therefore, the antenna needs to be optimized further to achieve wideband response. Design 2 shows a clearance of copper from the lower part of the ground plane. The bottom non ground portion of Antenna Design 2 is 7 × 100 mm<sup>2</sup>. This defect in the ground plane improved the impedance matching at lower bands (0.7 GHz, 1.2 GHz). At higher bands (2–4 GHz) the resonance bandwidth increases; however, the impedance matching becomes worse from 2 to 3.5 GHz as it can be seen in Fig. 5. Therefore, this design needs further optimization. This time copper is removed from the upper part of the ground plane in Design 3. Now, the top and bottom non ground portion of Design 3 is same i.e., 7 × 100 mm<sup>2</sup>. The S-parameters shown in Fig. 5 indicate that the impedance matching is not improved at higher resonances. Design 4 shows promising results after clearing more copper from the sides of the lower part of the ground plane. The side non ground portion of Design 4 is 15 × 23 mm<sup>2</sup> as shown in Fig. 4d. It can be seen from the S-parameter plots that two resonances are obtained at lower bands (0.76 GHz and 1.28 GHz) and a wideband performance is obtained at higher bands from 2.28 to 3.74 GHz. From Design 4, the proposed antenna is operating at UHF (0.755 GHz), L-band (1.25 GHz) and S-band (2.28–3.74 GHz), respectively. Table 1 shows the final optimized parameters of the proposed unit cell. The Fig. 5 explains the effect of different ground plane configurations on the antenna's impedance matching by comparing four design iterations (Design 1 to Design 4). As the ground plane's structure evolves, primarily through reducing copper coverage, the impedance matching improves significantly. Design 1, with a full ground plane, shows narrow bandwidth and poor matching, while Design 4, with reduced copper in the ground plane, achieves broader bandwidth and better impedance matching across the desired UHF, L, and S bands. This demonstrates that optimizing the ground plane is crucial for achieving wideband performance in the antenna design.

#### *Parametric study of proposed antenna*

Design 4 is further optimized using a parametric study. The height of the strip, H plays an important role in achieving good impedance matching at lower and higher frequency bands. After performing the parametric

sweep of different heights of the strip,  $H = 55$  mm is chosen as the optimum height in which lower and higher operating bands have reasonably good impedance matching below  $-15$  dB as shown in Fig. 6a. Subsequently, the connection to the ground point plays a crucial part, especially for the lower band compared to higher bands. This phenomenon can be seen in Fig. 6b. The optimized connection to the ground plane is obtained at 91 mm, which is the distance between the ground connecting patch and the bottom edge of the ground plane. Similarly, the feeding point is an important parameter in the proposed design. It affects the bandwidth of the operating bands,

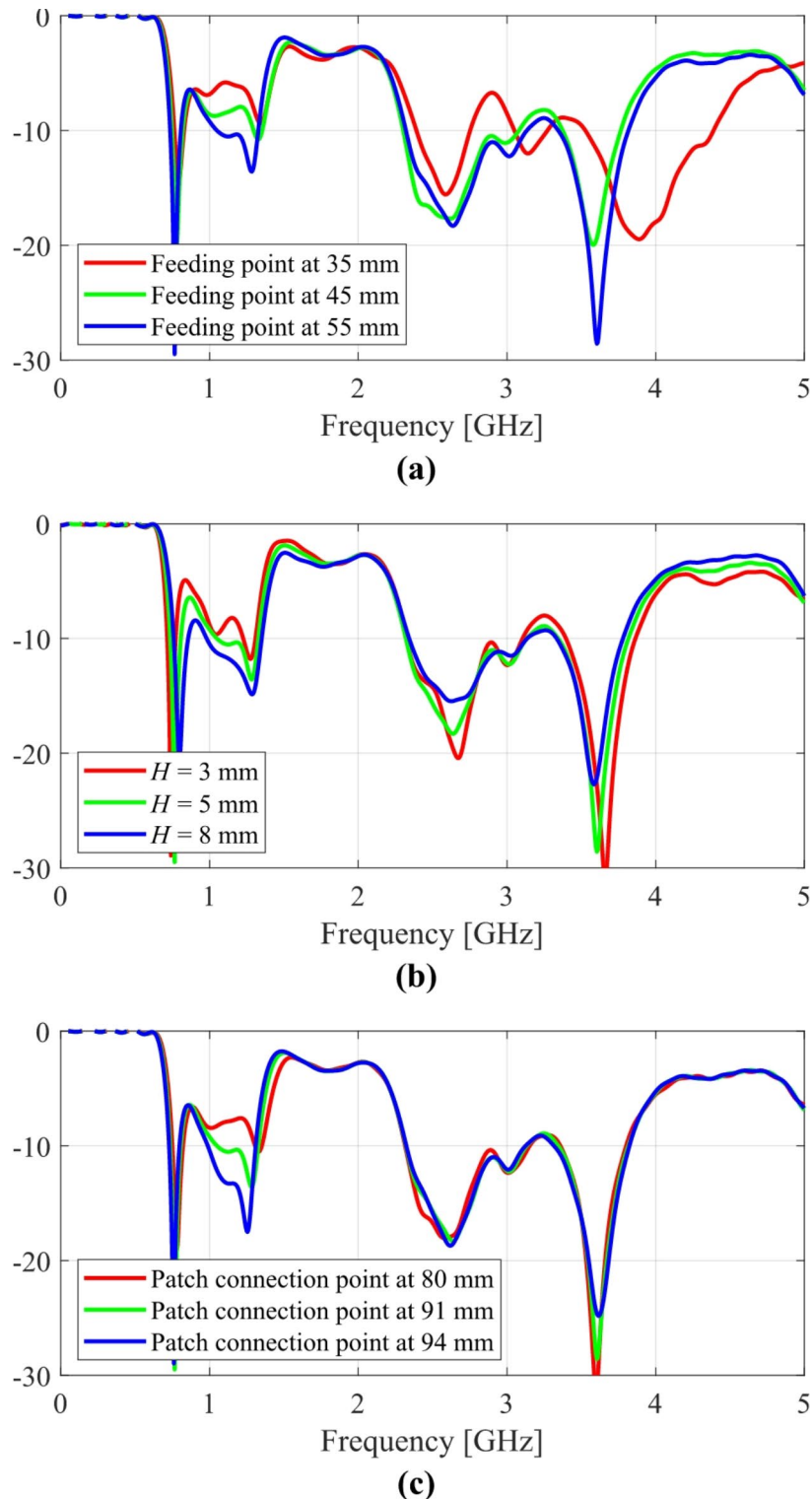


**Fig. 6.** Parametric Study of proposed antenna Design 4, (a) height,  $H$  of the metal strip, (b) patch connection point to ground plane, (c) feeding point.

especially in higher frequency bands. As can be seen in Fig. 6c. At different feeding points, the bandwidth of higher frequency bandwidth is affected. The optimized value is 55 mm of feeding point obtained upon analyzing the parametric study outcomes. Table 1 shows the final optimized parameters of the proposed antenna design.

### Vector surface current distribution

This section describes the vector surface current distribution of the proposed antenna design. It can be seen from the input impedance plot that there are five modes in total that resonate in proposed antenna where the imaginary part is zero as shown in Fig. 7. It shows that the final antenna with two loops produces five modes at 0.75 GHz, 1 GHz, 1.43 GHz, 1.85 GHz and 3.57 GHz. The surface current distributions for all modes are depicted in Fig. 8. The surface current distribution shows that the current is flowing in the upper region of the metal strip which is Loop 2 (IJKL). It contributed lower mode 1 which is the resonance frequency at 0.76 GHz as shown in Fig. 8a. Similarly, the surface current distribution shows the flow of current in the lower region of the antenna, which is defined by loop 1 (EFGH). It generates mode 2 at frequency 1 GHz as shown in Fig. 8b. Likewise, the surface current distributions indicate that at higher order modes the flow of current is within the entire antenna geometry. In some cases, the strong current flows near the feeding port and metal strip as shown in Fig. 8d and e, respectively. Also, a strong current flow can be seen near the connecting patch between the ground plane and the metal strip at the higher mode 3, cf. Fig. 8c.

Figure 9 illustrates the current distribution curve of the proposed antenna at various resonant frequencies, each corresponding to a specific mode. The current distribution varies across the antenna structure depending on the mode, revealing the areas of highest current concentration, which align with efficient radiation zones. At resonance, the current typically reaches its peak at specific points along the antenna structure. These areas with maximum current distribution indicate where the antenna is most efficient at radiating energy.

In Mode 1 (0.75 GHz), the current peaks in the lower metallic strip, demonstrating efficient operation in the UHF band. As the frequency increases to Mode 2 (1 GHz), the current spreads more evenly across both the metallic strip and the ground plane, indicating stronger resonance and broader coverage. At Mode 3 (1.43 GHz), the current covers a larger portion of the antenna structure, optimizing performance in the L-band, with significant current observed across both the upper and lower areas. In Mode 4 (1.85 GHz), the current is more focused around the feed port, which is crucial for enhancing power transfer and ensuring good radiation efficiency in this band. Finally, at Mode 5 (3.57 GHz), corresponding to the S-band, the current distribution covers the entire antenna structure, with the strongest current flows in critical areas like the metal strips, ensuring maximum radiation efficiency at higher frequencies. This mode-based analysis allows a clear understanding of how the antenna operates effectively across multiple frequency bands, from UHF to S-band, and highlights opportunities to further optimize the design for better performance.

### Antenna design with CubeSat

The proposed antenna is optimized and ready to be deployed inside the CubeSat. The CubeSat is designed using 3D printing. The underlying material is PLA plastic with relative permittivity 2.7. The size of the CubeSat is  $100 \times 100 \times 100 \text{ mm}^3$ . The CubeSat has been shown in Fig. 10. The antenna is placed at one face of the 3D printed CubeSat as can be seen in Fig. 8. The size of the ground plane with surrounded metal strips is  $102 \times 102 \times 5 \text{ mm}^3$ . The CubeSat has four more extensions of 2 mm from each side to tightly fix the surrounding metal strip. The proposed antenna consists of a ground plane and surrounding metallic strips, as described in the Antenna Geometry section. The ground plane is implemented on one side of the dielectric substrate, while the opposite side remains blank, ensuring efficient radiation characteristics. The metal strips, which are connected to the ground plane through vias, contribute to the multi-band resonance and omnidirectional radiation pattern.

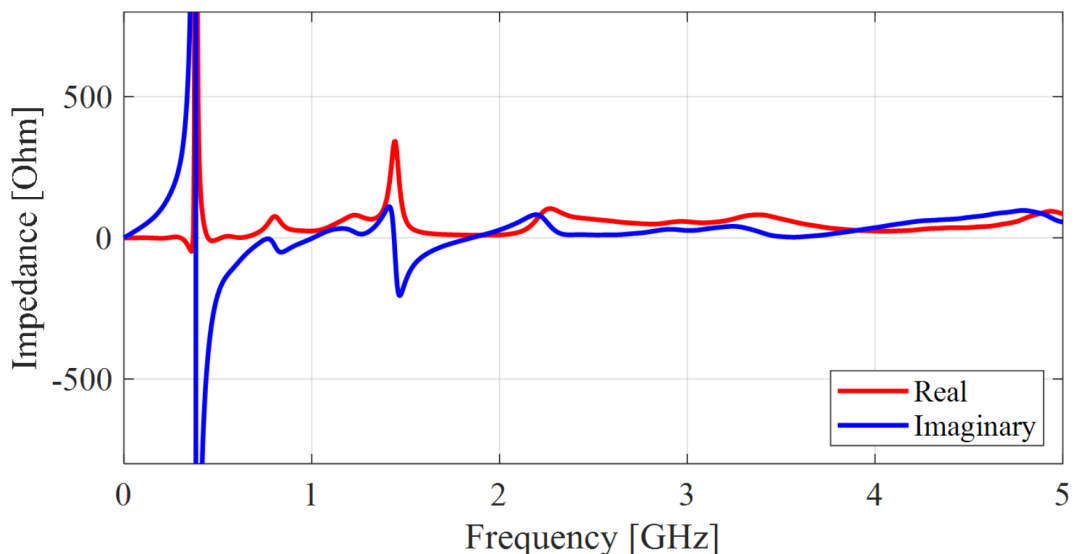
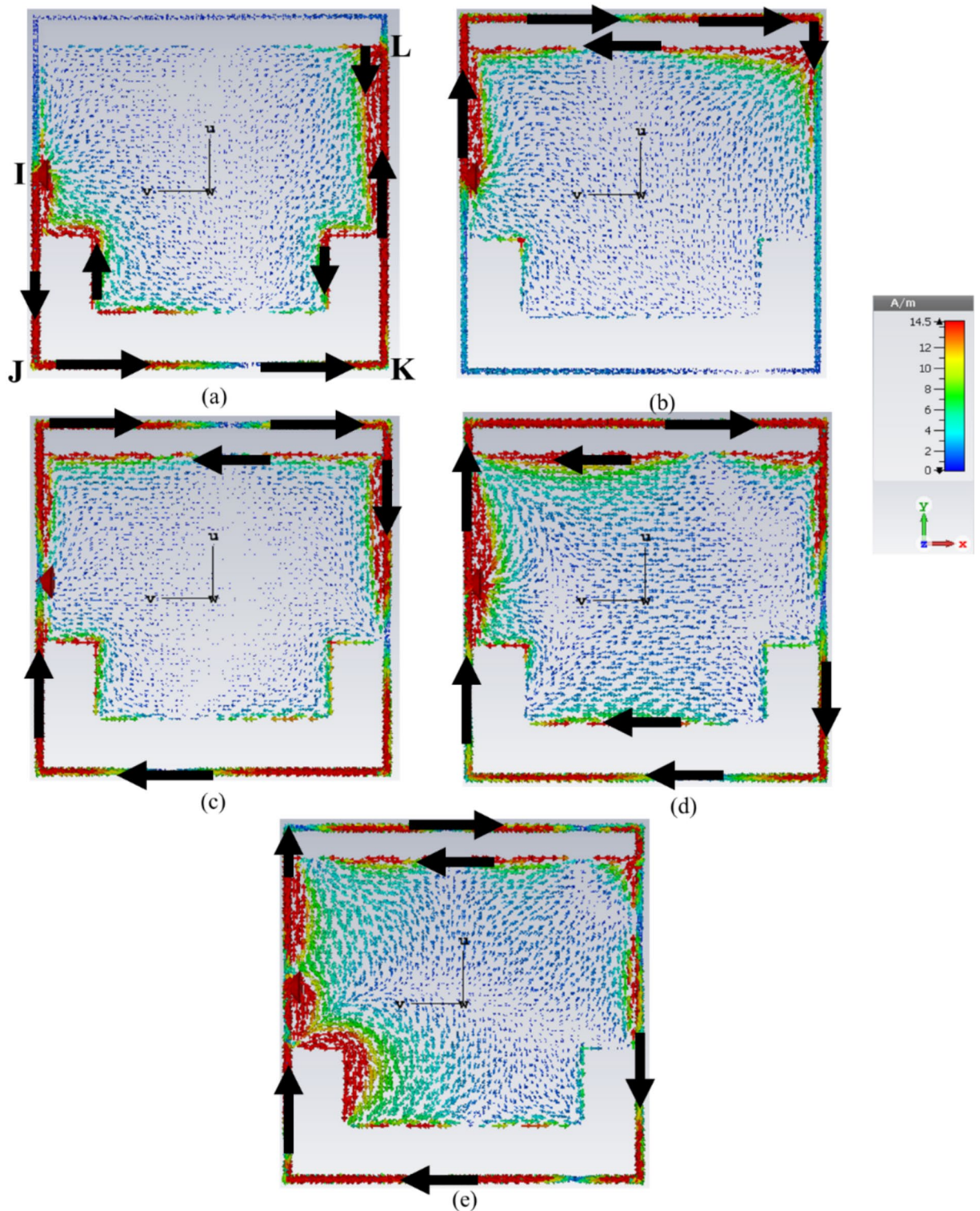


Fig. 7. Input impedance,  $Z$  of the proposed antenna.



**Fig. 8.** Vector surface current distribution within the proposed antenna: (a) Mode 1 at 0.75 GHz, (b) Mode 2 at 1 GHz, (c) Mode 3 at 1.43 GHz, (d) Mode 4 at 1.85 GHz and (e) Mode 5 at 3.57 GHz.

Regarding the impact of the CubeSat's metal structures, we acknowledge that the operational environment may introduce additional effects. The proposed antenna is perfectly fit inside the CubeSat occupying only  $100 \times 100 \times 0.508 \text{ mm}^3$ . Therefore, there is more room for placing payload, power and radio systems, solar panels, and flight control computer. Figure 11 shows the comparison of the S-parameters of the antenna with and without the CubeSat. It can be seen there is a little shift in frequency due to lossy plastic material of the CubeSat. However, the overall response of the proposed antenna is essentially the same.

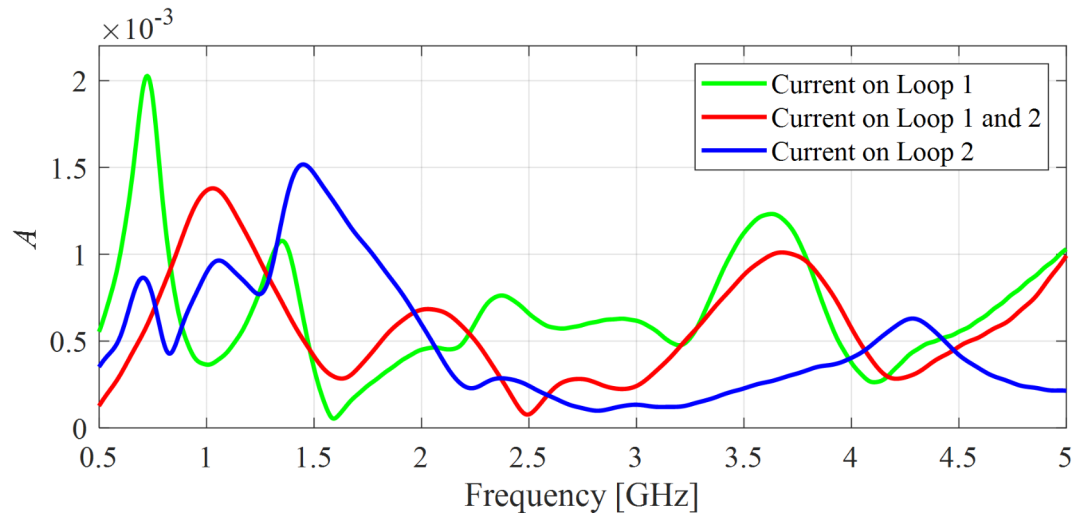


Fig. 9. Current distribution curves of the proposed antenna.

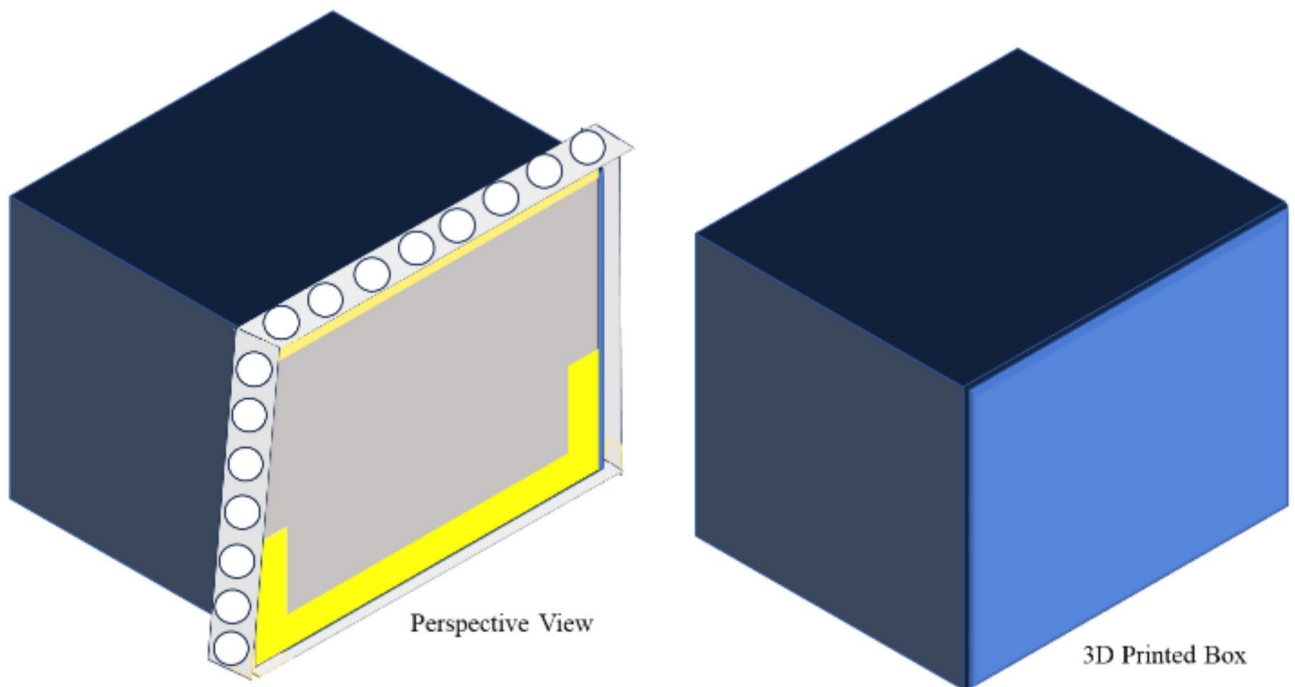


Fig. 10. 3D printed CubeSat and Proposed employed in a CubeSat.

### Antenna design 3D radiation pattern characteristics with/without CubeSat

The radiation characteristics of the proposed antenna are analyzed in this section. First, the 3D radiation characteristics of the antenna with and without CubeSat is investigated in terms of gain and radiation efficiency at resonant frequencies. The gain values are computed in a graph and reported in Fig. 12. The gain at all the frequencies is stable even if it evaluated inside the CubeSat, which shows the resilient feature of the proposed antenna design. Secondly, radiation efficiencies with and without CubeSat is plotted in Fig. 13. After incorporating the proposed antenna into the CubeSat, the antenna efficiency is degraded, however, the overall efficiency at all the resonant frequencies is above 90%.

### Experimental validation

The proposed antenna for CubeSat applications has been fabricated on Roger's RO4003 substrate. The CubeSat has been implemented using a 3D printer. The fabricated antenna is successfully deployed inside the CubeSat as shown in Fig. 14. The antenna ground plane is intentionally designed to be of the same size as the CubeSat, i.e.,  $100 \times 100 \text{ mm}^2$  to allocate the antenna at one of its faces. The surrounding metallic strips are separated exactly

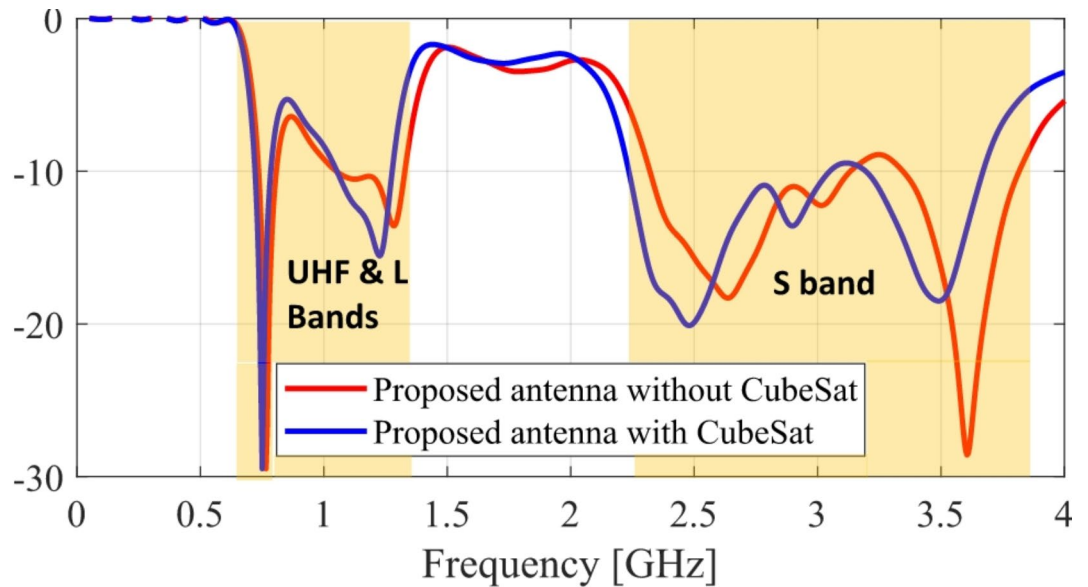


**Fig. 11.** Reflection response of the proposed antenna with and without CubeSat.

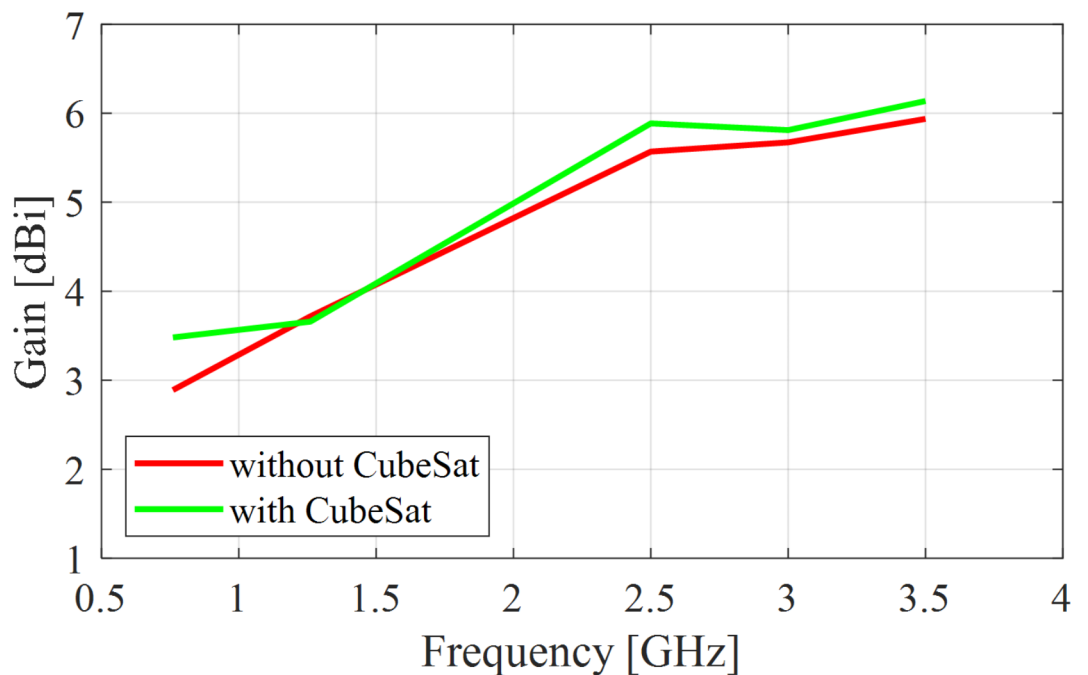


**Fig. 12.** Gain plot with and without CubeSat.

3 mm from the antenna's ground plane and the CubeSat, which is maintained by custom-made 3D extensions. Therefore, the metallic strips are rigid and easy to deploy. The coaxial connector and the connecting ground patch are soldered at the optimized location obtained from CST simulations. The overall weight of the antenna with CubeSat is low due to utilization of the plastic material.

The S-parameters of the proposed designs have been measured using the vector network analyzer. The simulated and measured reflection response as well as realized gain are plotted in Figs. 15 and 16, respectively. The alignment between the measurements and full-wave simulations is satisfactory. Minor discrepancies can be attributed to the connector and material losses. Figure 17 shows the experimental setup of the CubeSat antenna inside the anechoic chamber. The normalized directivity of the proposed array system is measured in the chamber at five frequencies, i.e., 0.75 GHz, 1.26 GHz, 2.5 GHz, 3 GHz, and 3.5 GHz. Figure 18 shows the radiation patterns at those frequencies. The figures illustrate the radiation patterns of the antenna at various frequencies—0.76 GHz, 1.26 GHz, 2.5 GHz, 3.0 GHz, and 3.5 GHz—comparing co-polarization (solid line) and



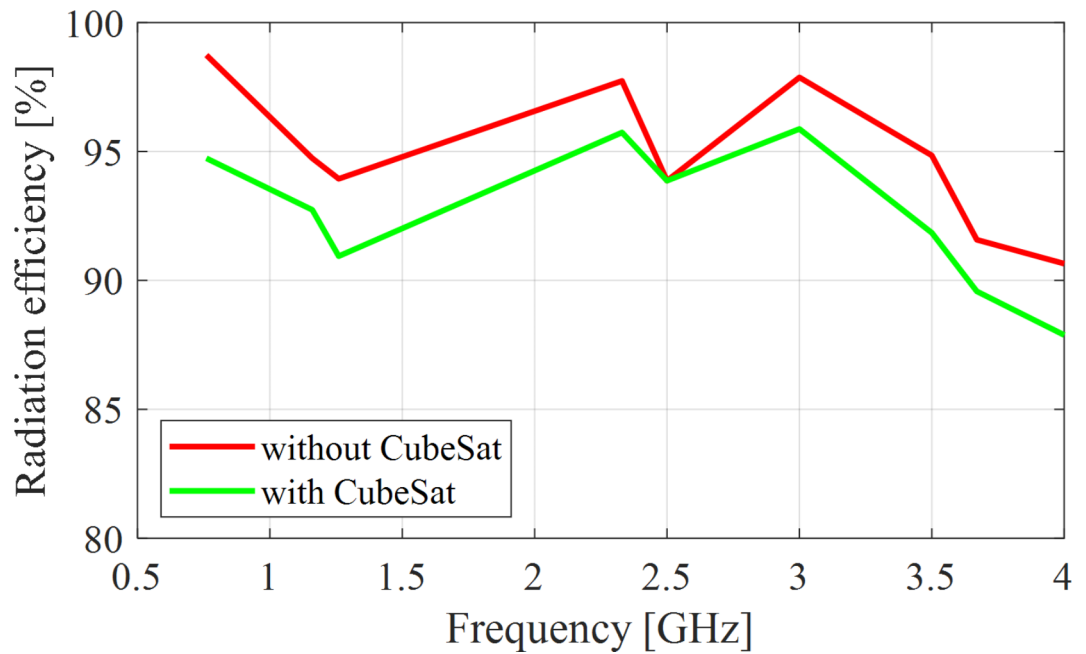


**Fig. 13.** Radiation Efficiency with and without CubeSat.



**Fig. 14.** Fabricated CubeSat antenna: (a) perspective view, (b) diverse side views.

cross-polarization (dashed line). At 0.76 GHz, the radiation pattern is uniform with low cross-polarization levels, indicating strong polarization purity. At 1.26 GHz, the pattern remains stable, with co-polarization showing significantly stronger radiation than cross-polarization, highlighting efficient performance at this frequency. At higher frequencies, such as 2.5 GHz, 3.0 GHz, and 3.5 GHz, the radiation patterns exhibit some variation, with a slight increase in cross-polarization, though the antenna maintains good polarization separation. These results demonstrate the antenna's ability to maintain consistent and effective radiation patterns across multiple frequencies, which is important for reliable communication in CubeSat applications.

Table 2 presents a comparison between the proposed antenna and different monopole and dipole antennas for CubeSat communications reported in the recent literature. The data presented in Table 2 indicates that the proposed structure exhibits a superior combination of bandwidth performance, triple operating bands (UHF, L and S) and compact size. The proposed antenna is easily deployable inside the CubeSat and offers a significant amount of room for other components such as solar panels, batteries, payloads etc. Furthermore, it features more operating bands with larger bandwidth as compared to other antennas. The antenna has a wide bandwidth especially at the S band around 1435 MHz, covering almost the entire band, which has not been demonstrated in the literature thus far. At the same time, it is considerable smaller than the benchmark structures of comparable other monopole/dipole antenna type.

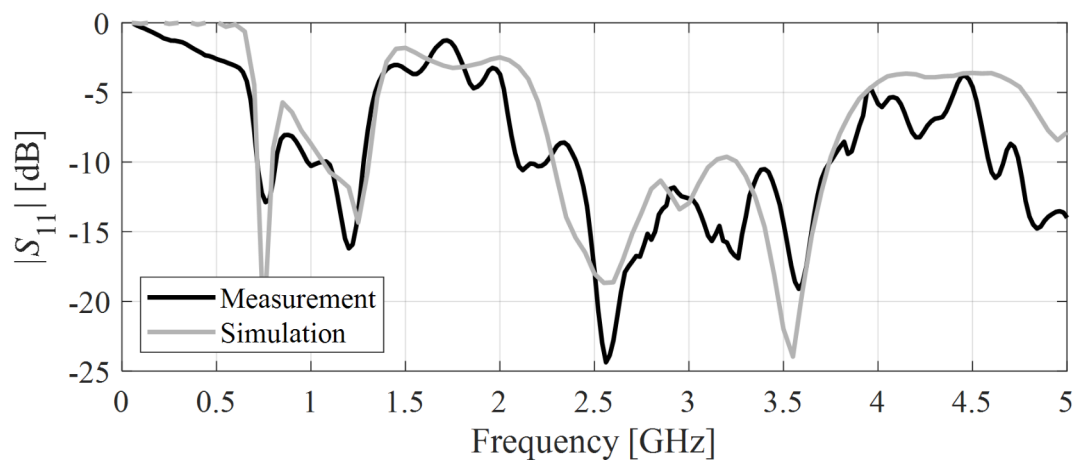


Fig. 15. Measured and simulated reflection response of the proposed antenna for CubeSat applications.

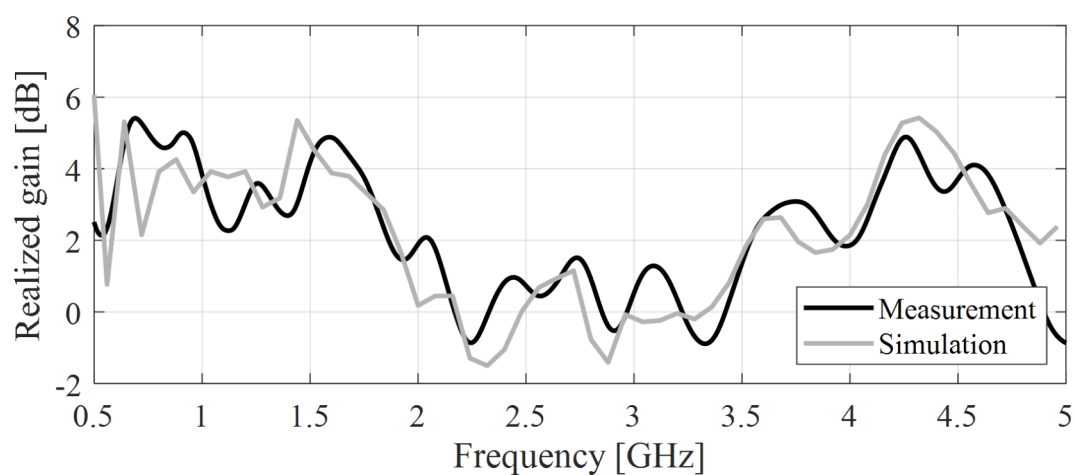


Fig. 16. Measured and simulated realized gain (maximum within the  $yz$ -plane).

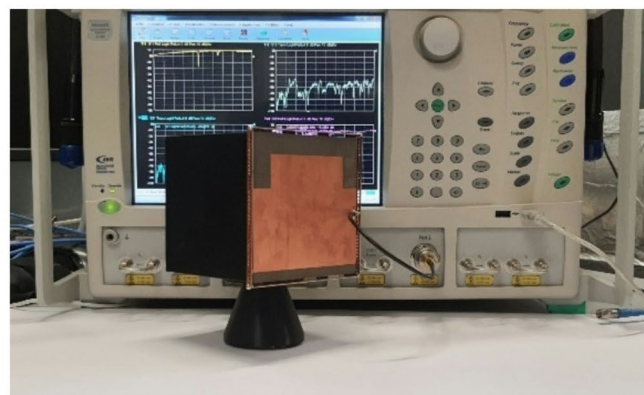
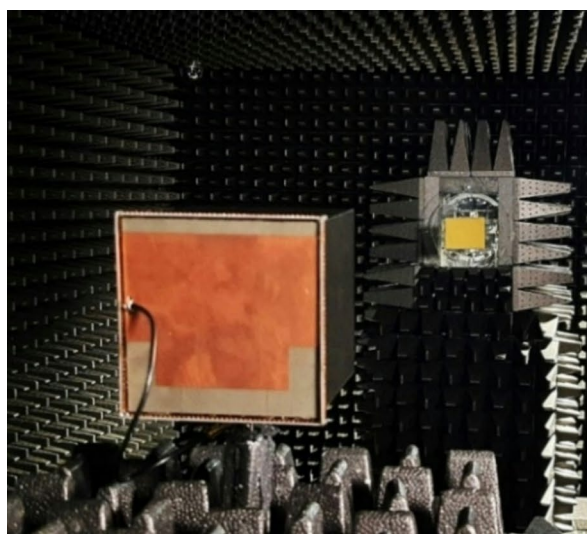
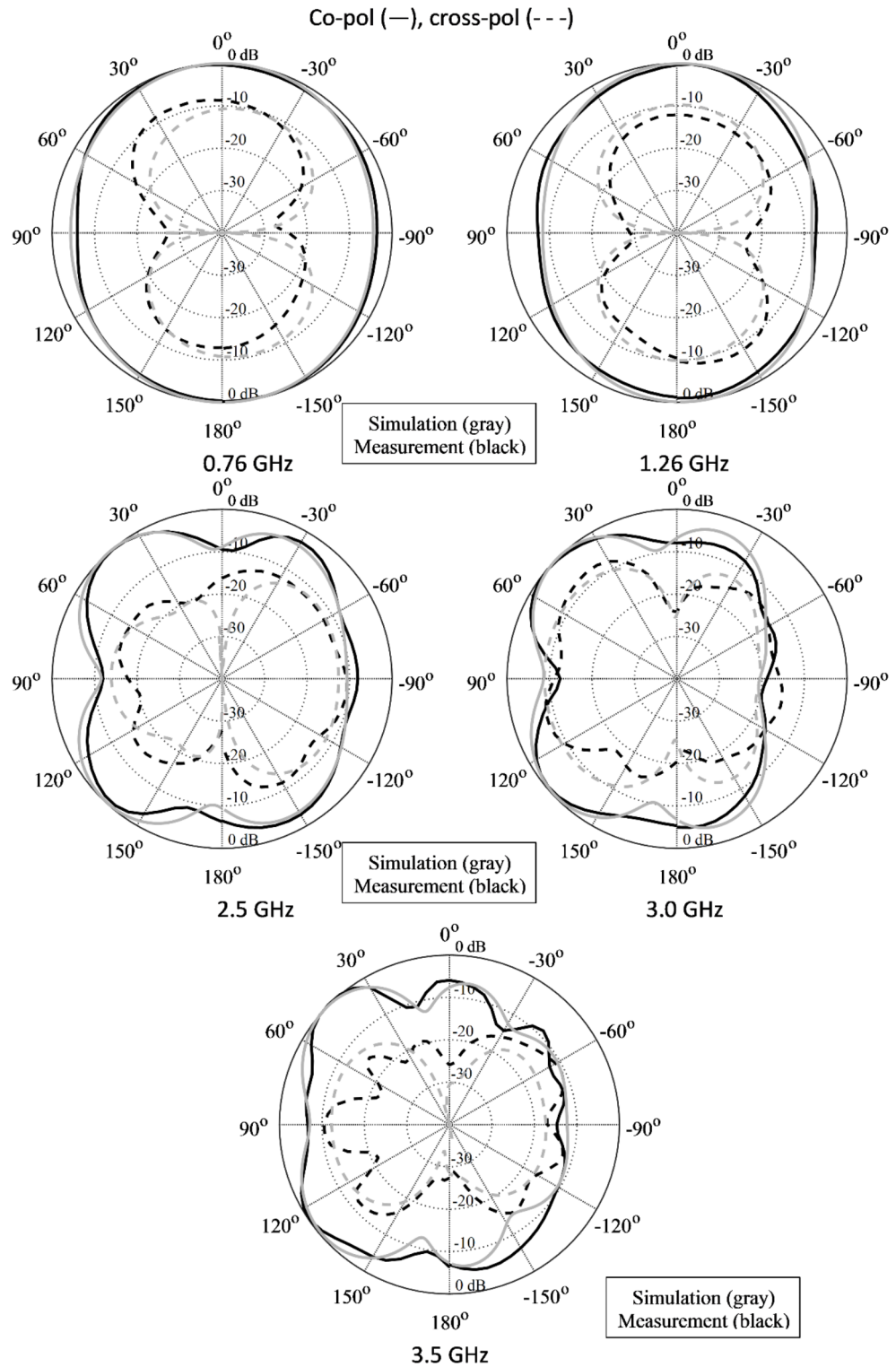


Fig. 17. Measurement setup for CubeSat antenna.



**Fig. 18.** Radiation patterns at 0.75 GHz, 1.26 GHz, 2.5 GHz, 3 GHz, and 3.5 GHz. Co- and cross-pol marked using solid and dashed lines, respectively. Simulation and measurement marked using grey and black lines, respectively.

**Proposed CubeSat possible application**

Satellite-based air traffic monitoring is evolving with the integration of CubeSats, small and cost-effective satellites that play a key role in improving global aviation safety. CubeSats are miniaturized satellites that provide a more affordable and accessible option for monitoring air traffic, complementing the existing satellite systems. Incorporating CubeSats into air traffic monitoring systems allows for additional layers of communication

References	Antenna size (in terms of $\lambda$ )	Operating Frequency (GHz)	10 dB Bandwidth (MHz)	Gain (dBi)	Antenna type	Deployable	CubeSat Type	Radiation efficiency (%)
3	$0.6\lambda \times 0.53\lambda$	15 (Ku-band)	14,800–1510	8.41	SIW Cavity Backed Antenna	Yes	IU	N.A
4	$2.6\lambda \times 2.6\lambda$	7.75–8.75 (X-band)	8025–8400	18.65	$4 \times 4$ Array	No	IU	60 to 82
6	N. A	5.8 (C-band)	N. A	23.6	$17 \times 17$ Array	Yes	N. A	N. A
7	$0.048\lambda \times 0.048\lambda \times 0.004\lambda$	8 (X-band)	6100–13,900	7.3	$5 \times 5$ Array	No	N. A	N. A
9	$0.87\lambda \times 0.87\lambda \times 0.042\lambda$	2.5 (S-band), 4.7 (C-band)	2250–2750, 4575–4825	7.55, 4.9	Folded-end Dipole	Yes	IU	N. A
27	$0.13\lambda \times 0.05\lambda \times 0.011\lambda$	1st 0.398 (UHF-band), 2nd 0.149 (VHF-band)	142.5–155.5, 393–403	1.72, 3.11	Monopole	Yes	N. A	N. A
32	$0.66\lambda \times 0.66\lambda$	2.5 (S-band)	2440–2560	5.03	Printed Dipole	No	IU	N. A
33	$0.45\lambda \times 0.45\lambda$	2.45 (S-band)	2050–2870	3.49	Printed Dipole	No	IU	N. A
34	$0.015\lambda \times 0.048\lambda$	0.144 (VHF), 0.435 (UHF) 0.144 (VHF), 0.435 (UHF)	N. A	2.59 3.91 2.14 4.35	Dipole Monopole	Yes	IU	N. A
This work	$0.26\lambda \times 0.26\lambda \times 0.013\lambda$	0.755 (UHF), 1.25 (L-band), and 2.28 to 3.74 (S-band)	710–790, 1040–1290, 2230–3680	3.12, 3.2, 5.2	Monopoles	Yes	IU	90

**Table 2.** Performance comparison between proposed antenna and state-of-the-art designs.

and tracking, particularly in remote or underserved regions. These CubeSats can be equipped with GPS receivers, communication systems, and data relay capabilities, extending the coverage of air traffic monitoring beyond traditional satellites. Due to their small size and lower launch cost, CubeSats can be deployed in large constellations, enhancing global coverage and providing more frequent data updates. The proposed CubeSat antenna application can serve this purpose but is not limited to it. As shown in Fig. 19, CubeSats work in tandem with communication satellites, GPS satellites, and aircraft-to-aircraft data exchange systems. CubeSats can serve as relay stations, helping aircraft transmit Automatic Dependent Surveillance–Broadcast (ADS-B) signals even in areas with poor or no traditional radar coverage, such as oceans and polar regions. The data collected by CubeSats, including precise positioning from GPS, is transmitted back to ground stations for real-time analysis, improving flight path accuracy, situational awareness, and overall safety. By combining CubeSat technology with existing satellite-based systems, air traffic monitoring becomes more robust, scalable, and cost-efficient, ensuring continuous and optimized aircraft tracking, reduced congestion, and improved communication across the global airspace.

### Benchmarking

The proposed antenna design offers significant advancements over existing CubeSat antennas, as demonstrated in Table 2. Unlike conventional CubeSat antennas that primarily operate in a single or dual-band configuration, our design introduces a compact tri-band omnidirectional antenna that covers UHF, L-band, and S-band, ensuring broader frequency utilization for satellite communication. One of the key innovations of this work is the integration of a defected ground structure (DGS) and metallic vias, which enhances impedance matching and enables stable multi-band resonance without the need for complex matching networks. Additionally, the antenna is fully enclosed within a 1U CubeSat and does not require external deployment, making it mechanically robust and easy to integrate within small satellite platforms. The omnidirectional radiation pattern ensures consistent connectivity between the CubeSat and ground stations, even in dynamic orientations. Furthermore, the antenna exhibits high radiation efficiency (above 90%), outperforming several state-of-the-art CubeSat antennas with high material and impedance mismatch losses. Experimental validation, including fabricated prototype measurements and anechoic chamber testing, confirms the accuracy of simulated results, demonstrating reliable performance in real-world CubeSat conditions. Compared to existing monopole and dipole CubeSat antennas, our design provides better bandwidth, higher radiation efficiency, and a more compact form factor, making it an ideal candidate for the next-generation CubeSat communication systems.

### Conclusion

This work presented a compact tri-band omnidirectional antenna optimized for 1U CubeSat applications, offering stable performance across UHF, L, and S-bands. The design incorporates metallic vias and a defected ground structure (DGS) to achieve multi-band resonance and high radiation efficiency, exceeding 90% at all resonance frequencies. The antenna's small footprint ( $102 \times 102 \times 5 \text{ mm}^3$ ) and fully enclosed structure eliminates the need for external deployment, making it easy to integrate within CubeSat platforms while leaving ample room for other critical components. Experimental validation, including fabrication and anechoic chamber testing, confirms the antenna's cutting edge performance alignment between simulated and measured results. Compared to existing CubeSat antennas, the proposed design offers better bandwidth, higher radiation efficiency, and a more compact structure, making it an ideal solution for next-generation low-cost, high-performance CubeSat communication systems.

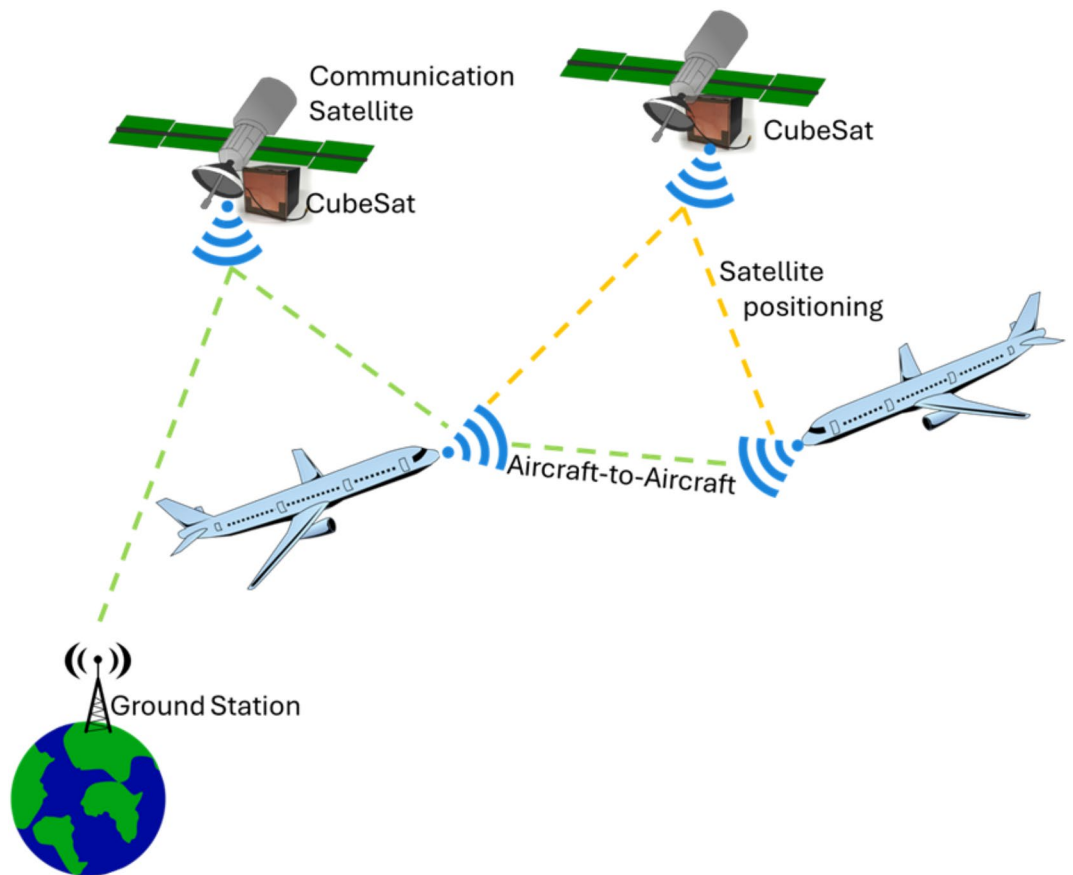


**Fig. 19.** Possible implementation of satellite and CubeSat-based air traffic monitoring system in aviation networks.

### Data availability

The datasets generated during and/or analysed during the current study are available from the corresponding author on reasonable request.

Received: 24 December 2024; Accepted: 31 March 2025

Published online: 07 April 2025

### References

- Karl, B.-H., The Future of CubeSats. Accessed August 15, 2014; <https://www.nasa.gov/missions/the-future-of-cubesats/>.
- Laura, W., Insights on the CubeSat Global Market to 2027—Increase in Demand for Space Data Presents Opportunities: Research and Markets. Accessed April 08, 2021; <https://www.globenewswire.com/en/news-release/2021/04/08/2206504/28124/en/Insights-on-the-CubeSat-Global-Market-to-2027-Increase-in-Demand-for-Space-Data-Presents-Opportunities.html>.
- De, R., Abegaonkar, M. P. & Basu, A. Compact dual slot SIW cavity backed antenna for CubeSat/nanosatellite applications. *IEEE Access* **11**, 78802–78810 (2023).
- Hester, D., Han, S. & Adams, M. Design methodology for single-feed circularly polarized X-band antenna arrays for CubeSats using multilevel sequential rotation. *IEEE J. Miniatur. Air Spac Syst.* **5**, 42–50 (2024).
- Mahmoud, M. N. & Baktur, R. Integrated solar panel slot antennas certified for CubeSat missions. *IEEE Open J. Ant. Propag.* **5**, 686–692 (2024).
- Machida, M., Tomura, T., Sakamoto, H. & Fukao, T. Stretchable-substrate-impregnated fabric: Deployable reflectarray antennas for CubeSats. *IEEE Access* **12**, 58562–58572 (2024).
- Hammoui, M. E. et al. A Wideband circularly polarized CPW-Fed printed monopole X-band antenna for CubeSat applications. *IEEE Access* **11**, 121077–121086 (2023).
- Willis, J., Walton, P., Wilde, D. & Long, D. Miniaturized solutions for CubeSat servicing and safety requirements. *IEEE J. Miniatur. Air Space Syst.* **1**, 3–9 (2020).
- Liu, S., Raad, R., Theoharis, P. I. & Tubbal, F. Dual-band folded-end dipole antenna for plastic CubeSats. *IEEE J. Miniatur. Air Space Syst.* **1**, 172–178 (2020).
- Abulgasem, S. et al. Antenna designs for CubeSats: A review. *IEEE Access* **9**, 45289–45324 (2021).
- Saeed, N. et al. CubeSat communications: Recent advances and future challenges. *IEEE Comm. Surveys Tutor.* **22**, 1839–1862 (2020).
- Tubbal, F. E., Raad, R. & Chin, K.-W. A survey and study of planar antennas for pico-satellites. *IEEE Access* **3**, 2590–2612 (2015).
- Rahmat-Samii, Y., Manohar, V. & Kovitz, J. M. For satellites, think small, dream big: A review of recent antenna developments for CubeSats. *IEEE Antennas Propag. Mag.* **59**, 22–30 (2017).
- Wikipedia. F-1 (satellite). Accessed 2022, Aug 21; [https://en.wikipedia.org/wiki/F-1\\_\(satellite\)](https://en.wikipedia.org/wiki/F-1_(satellite)).

15. Chahat, N., Sauder, J., Thomson, M., Hodges R., and Rahmat-Samii, Y. CubeSat deployable Ka-band reflector antenna for deep space missions. In *Proc. IEEE Int. Symp. Antennas and Propagation and U.S. Nat. Committee/Int. Union Radio Sci. Nat. Radio Science Meeting*, 2185–2186 (2015).
16. State of the Art of Small Spacecraft Technology. <https://sst-soa.arc.nasa.gov/03-power>.
17. Warren, P. A., Steinbeck, J. W., Minelli, R. J. & Mueller, C. Large, deployable S-band antenna for a 6U CubeSat. In *Proc. 29<sup>th</sup> Annu. American Inst. Aeronautics and Astronautics/Utah State University Conf. Small Satellites*, 1–7 (2015).
18. King, A., Ness, J., Bonin, G., Brett, M. & Faber, D. Nanosat Ka-band communications: A paradigm shift in small satellite data throughput. In *Proc. 26<sup>th</sup> American Inst. Aeronautics and Astronautics/Utah State University Conf. Small Satellites*, 1–21 (2012).
19. Magalhaes, M. P., Heckler, M. V., Mota, J., Sombra, A. S. & Moreira, E. C. Design and analysis of microstrip antenna arrays for meteorological nanosatellites for UHF uplink. In *Proc. Int. Telecommunications Symp.*, 1–5(2014).
20. Jarchavi, S. M. R., Hussain, M., Gardezi, S. H. H., Alibakhshikenari, M., Falcone, F. & Limiti, E. A Compact and Simple Prototype CPW-Fed Dual Band Antenna for ISM, Wi-Fi, and WLAN Applications. In *United States National Committee of URSI National Radio Science Meeting (USNC-URSI NRSM)*, Boulder, CO, USA, 30–31 (2022).
21. Hussain, M., Rizvi, S. N. R., Shaikat, H., Alibakhshikenari, M., Falcone, F. & Limiti, E. Broad-Band Miniaturized Antenna Implementation Working Among 57–70 GHz V-Band for 5th Generation and Beyond Applications. In *46<sup>th</sup> International Conference on Infrared, Millimeter and Terahertz Waves (IRMMW-THz)*, Chengdu, China, 1–2 (2021).
22. Awan, W. A. et al. A low profile frequency reconfigurable antenna for mmWave applications. In *WITS 2020. Lecture Notes in Electrical Engineering* Vol. 745 (eds Bennani, S. et al.) (Springer, Singapore, 2022).
23. Hussain, M., Rafique, U., Dalal, P., Abbas, S. M. & Zhu, Y. A Compact and Wide Band Antenna for Millimeter Wave Applications. In *IEEE Wireless Antenna and Microwave Symposium (WAMS)*, Visakhapatnam, India, 1–4 (2024).
24. Hussain, M., Rafique, U., Zahra, H., Abbas, S. M., and Mukhopadhyay, S. A Compact and Geometrically Simple CPW Fed Antenna for 2.4/5.4 GHz ISM and WLAN Applications. In *IEEE International Symposium on Antennas and Propagation and USNC-URSI Radio Science Meeting (USNC-URSI)*, Portland, OR, USA, 1199–1200 (2023).
25. Shah, P. and Kumar, S. A Circularly Polarized Swastika Shaped Crossed Dipole Antenna for Cubesat. In *2021 IEEE 8<sup>th</sup> Uttar Pradesh Section Inter. Conf. on Elect., Electro. & Comp. Eng. (UPCON)*, 1–4 (2021).
26. Govindarajan, H. et al. Design of a compact dual circular-polarized antenna for L-band satellite applications. *IEEE Ant. Wire. Propa. Lett.* **19**, 547–551 (2020).
27. Zhang, X., Sun, F., Zhang, G. & Hou, L. Compact UHF/VHF monopole antennas for CubeSats applications. *IEEE Access* **8**, 133360–133366 (2020).
28. Schraml, K., Narbudowicz, A., Chalermwisutkul, S., Heberling, D. and Ammann, M. J. Easy-to-deploy LC-loaded dipole and monopole antennas for CubeSat. In *Proc. 11<sup>th</sup> Eur. Conf. Antennas Propag. (EUCAP)*, 2303–2306 (2017).
29. Piattoni, J., Candini, G. P., Pezzi, G., Santoni, F. & Piergentili, F. Plastic Cubesat: An innovative and low-cost way to perform applied space research and hands-on education. *Acta Astronaut.* **81**, 419–429 (2012).
30. Rochus, P. et al. New applications of rapid prototyping and rapid manufacturing (RP/RM) technologies for space instrumentation. *Acta Astronaut.* **61**, 352–359 (2007).
31. CST Microwave Studio, Dassault Systemes, France, 2020. Link: CST STUDIO SUITE Learning Edition | 3DEXPERIENCE Edu – Dassault Systèmes (3ds.com)
32. Liu, S., Raad, R., Chin, K. -W. & Tubbal, F. E. M. Dipole antenna array cluster for CubeSats. In *10<sup>th</sup> Inter. Conf. on Signal Proc. & Comm. Sys. (ICSPCS)*, 1–4 (2016).
33. Lokman, A. H. et al. Compact circularly polarized S-band antenna for pico-satellites. In *Inter. Symp. on Ant. & Prop. (ISAP)*, 1–2 (2017).
34. Schraml, K., Narbudowicz, A., Chalermwisutkul, S., Heberling, D. & Ammann, M. J. Easy-to-deploy LC-loaded dipole and monopole antennas for cubesat. In *11<sup>th</sup> Euro. Conf. on Ant. & Prop. (EUCAP)*, 2303–2306 (2017).

## Acknowledgements

The authors would like to thank Dassault Systemes, France, for making CST Microwave Studio available. This work was supported in part by the Icelandic Research Fund Grant 217771, and by the National Science Centre of Poland Grant 2022/47/B/ST7/00072.

## Author contributions

Conceptualization, R.S.A.; methodology, R.S.A. and S.K.; software, A.P., S.K. and R.S.A.; validation, A.P., S.K. and R.S.A.; formal analysis, R.S.A.; investigation, R.S.A. and S.K.; resources, A.P. and S.K.; data curation, S.K. and R.S.A.; writing—original draft preparation S.K. and R.S.A.; writing—review and editing, A.P. and S.K.; visualization, A.P., S.K. and R.S.A.; supervision, S.K.; project administration, S.K.; funding acquisition, A.P. and S.K. All authors reviewed the manuscript.

## Declarations

## Competing interests

The authors declare no competing interests.

## Additional information

**Correspondence** and requests for materials should be addressed to R.S.A.

**Reprints and permissions information** is available at [www.nature.com/reprints](http://www.nature.com/reprints).

**Publisher's note** Springer Nature remains neutral with regard to jurisdictional claims in published maps and institutional affiliations.

**Open Access** This article is licensed under a Creative Commons Attribution-NonCommercial-NoDerivatives 4.0 International License, which permits any non-commercial use, sharing, distribution and reproduction in any medium or format, as long as you give appropriate credit to the original author(s) and the source, provide a link to the Creative Commons licence, and indicate if you modified the licensed material. You do not have permission under this licence to share adapted material derived from this article or parts of it. The images or other third party material in this article are included in the article's Creative Commons licence, unless indicated otherwise in a credit line to the material. If material is not included in the article's Creative Commons licence and your intended use is not permitted by statutory regulation or exceeds the permitted use, you will need to obtain permission directly from the copyright holder. To view a copy of this licence, visit <http://creativecommons.org/licenses/by-nc-nd/4.0/>.

© The Author(s) 2025